

2015

Numerical Investigation of Pressure Drop and Heat Transfer through Reconstructed Metal Foams and Comparison against Experiments

A. Diani

Università degli Studi di Padova

K. K. Bodla

General Electric

L. Rosetto

Università degli Studi di Padova

S V. Garimella

Purdue University, sureshg@purdue.edu

Follow this and additional works at: <http://docs.lib.purdue.edu/coolingpubs>

Diani, A.; Bodla, K. K.; Rosetto, L.; and Garimella, S V., "Numerical Investigation of Pressure Drop and Heat Transfer through Reconstructed Metal Foams and Comparison against Experiments" (2015). *CTRC Research Publications*. Paper 258.
<http://dx.doi.org/10.1016/j.ijheatmasstransfer.2015.04.038>

This document has been made available through Purdue e-Pubs, a service of the Purdue University Libraries. Please contact epubs@purdue.edu for additional information.

Article to be submitted to

INTERNATIONAL JOURNAL
OF HEAT AND MASS TRANSFER

Title

Numerical Investigation of Pressure Drop and Heat Transfer through Reconstructed
Metal Foams and Comparison against Experiments

Authors

Andrea Diani¹, Karthik K. Bodla², Luisa Rossetto¹, Suresh V. Garimella²

Affiliation

¹Dipartimento di Ingegneria Industriale, Università degli Studi di Padova, Via Venezia 1, 35131,
Padova, Italy.

²School of Mechanical Engineering, Purdue University, 585 Purdue Mall, West Lafayette, IN
47907-2088, United States

Corresponding Author

Prof. Luisa Rossetto,

Dipartimento di Ingegneria Industriale

Università degli Studi di Padova,

Via Venezia 1, 35131 Padova – ITALY

Ph. +39 049 8276869

Fax. +39 049 8276896

email: luisa.rossetto@unipd.it

Highlights:

- μ CT scanning and geometric reconstruction of copper foam samples.
- Fluid flow and heat transfer simulations on geometrically faithful reconstructions for forced convection of air through copper foams.
- Comparison of simulation results against experimental pressure gradients and empirical interstitial heat transfer coefficients.

ABSTRACT

Direct numerical simulation of transport in foam materials can benefit from realistic representations of the porous-medium geometry generated by employing non-destructive 3D imaging techniques. X-ray microtomography employs computer-processed X-rays to produce tomographic images or slices of specific regions of the object under investigation, and is ideally suited for imaging opaque and intricate porous media. In this work, we employ micro-CT for numerical analysis of air flow and convection through four different high-porosity copper foams. All four foam samples exhibit approximately the same relative density (6.4% - 6.6% solid volume fraction), but have different pore densities (5, 10, 20, and 40 pores per inch, PPI). A commercial micro-computed tomography scanner is employed for scanning the 3D microstructure of the foams at a resolution of 20 μm , yielding stacks of two-dimensional images. These images are processed in order to reconstruct and mesh the real, random structure of the foams, upon which simulations are conducted of forced convection through the pore spaces of the foam samples. The pressure drop values from this μCT based CFD analysis are compared against prior experimental results; the computational interfacial heat transfer results are compared against the values predicted by an empirical correlation previously reported, revealing excellent agreement between the numerical and experimental/empirical hydraulic and thermal results, thus highlighting the efficacy of this novel approach.

Keywords: microtomography, metal foams, pore scale simulation, pressure drop, heat transfer coefficient, forced air convection, electronics cooling.

NOMENCLATURE

a_{sv}	surface area per unit of volume [$\text{m}^2 \text{m}^{-3}$]
c_p	specific heat at constant pressure [$\text{J kg}^{-1} \text{K}^{-1}$]
e_A	absolute deviation [%]
e_R	relative deviation [%]
G	mass velocity [$\text{kg m}^{-2} \text{s}^{-1}$]
H	foam core height [m]
m	parameter defined in equation 8 [m^{-1}]
l	fiber length [m]
L	parameter defined in equation 9 [m]
p	pressure [Pa]
Pr	Prandtl number [-]
q''	heat flux [W m^{-2}]
Re	Reynolds number [-]
t	fiber thickness [m]
T	temperature [K]
\bar{T}_{air}	mean air temperature [K]
\bar{T}_{wall}	mean wall temperature [K]
u_i	velocity in the i -direction [m s^{-1}]
u_j	velocity in the j -direction [m s^{-1}]
x_i	coordinate in the i -direction [m]
x_y	coordinate in the y -direction [m]

Greek symbols

α	heat transfer coefficient [$\text{W m}^{-2} \text{K}^{-1}$]
$\alpha_{\text{empirical}}$	empirical heat transfer coefficient [$\text{W m}^{-2} \text{K}^{-1}$]
$\alpha_{\text{numerical}}$	numerical interfacial heat transfer coefficient [$\text{W m}^{-2} \text{K}^{-1}$]
ε	porosity [-]
λ_{air}	air thermal conductivity [$\text{W m}^{-1} \text{K}^{-1}$]
λ_{mat}	foam material thermal conductivity [$\text{W m}^{-1} \text{K}^{-1}$]
μ	dynamic viscosity [Pa s]

ρ	density [kg m ⁻³]
σ_N	standard deviation [%]
Ω^*	foam finned surface efficiency [-]

1. INTRODUCTION

Open-celled metal foams are a network of randomly oriented ligaments, consisting of connected pores with nearly uniform size and shape. These foam structures have several beneficial heat transfer characteristics, such as a large surface area per unit volume, high thermal conductivity, and enhanced flow mixing capabilities [1, 2]. These desirable, multi-functional characteristics make foams suitable extended surfaces for diverse applications such as air conditioning, refrigeration, and electronic cooling. Metal foams are primarily characterized by two parameters, *viz.*, the volumetric porosity denoted by ε , which is defined as the ratio of total void volume to cumulative volume occupied by the solid matrix and void space, and the number of pores per linear inch (PPI).

Much of the work in literature on heat transfer through metal foams has been focused on single phase flow. Similarly, a majority of the literature views foam structures as an alternative extended surface (*i.e.*, fins) using air as the coolant. Examples of experimental studies on forced convection of air through metal foams include those by Younis and Viskanta [3], Hwang *et al.* [4], Hsieh *et al.* [5], Duckhan and Chen [6], Incera Garrido *et al.* [7], Mancin *et al.* [2, 8], and Zhao [1]. Among these studies, Mancin *et al.* [2] reported heat transfer and pressure drop measurements performed for forced convection of air through multiple copper foam samples. The sample space investigated consisted of PPI values in the range 5 to 40, and porosity values in the range 0.905 to 0.934. The effect of different geometrical parameters of the foam on the global heat transfer coefficient, normalized mean wall temperature, pressure gradient, permeability, inertia coefficient, and drag coefficient were described. Zhao [1] provided a review on several thermal transport mechanisms in open-celled foams including conduction, forced convection, natural convection, thermal radiation, as well as pool boiling and flow boiling heat transfer. Very few researchers had focused on detailed heat transfer analysis at the pore scale, either by numerical or experimental approaches.

Traditional approaches of modeling fluid and thermal transport through metal foams approximate stochastic foams as periodic porous materials, and employ a single unit cell for analysis. Lu *et al.* [9] developed a simple analytical model to evaluate the utility of metal foams as compact heat exchangers. A cubic unit cell model consisting of slender cylinders as edges was developed to capture the most important trends of energy flow due to forced convection, and conduction through cell ligaments of the cellular foam.

Boomsma *et al.* [10] modeled the fluid flow through porous media with periodic unit cells. The energy minimization tool, Surface Evolver [11], was employed to obtain the microstructure of the foam. The pressure drops from the numerical simulations were compared against previous

experimental results of Boomsma and Poulikakos [12]. Under identical conditions, it was reported that the pressure drop values predicted by the simulations were consistently approximately 25% lower than the experimental values, and this underestimation was attributed to the exclusion of the bounding wall effects which would increase the pressure drop.

Krishnan *et al.* [13] performed direct numerical simulation of thermal transport through open-celled foams using different periodic unit cell geometries. They used three packaging arrangements of spheres, *viz.*, body centered cubic, face centered cubic and A15 lattice, to model the structure of the foams. Important thermal and hydraulic properties such as effective thermal conductivity, pressure drop and Nusselt number were computed for aluminum foams with both air and water as the interstitial fluid, and the results were successfully compared against experimental values and semi-empirical models available in the literature.

Annappagada *et al.* [14] proposed a computational method to analyze fluid flow and heat transfer in compressed open-celled metal foams. Their unit cells were similar to those considered by Krishnan *et al.* [13]: body centered cubic, face centered cubic, and A15. They first validated the results for the A15 model by comparing the normalized permeability of compressed polyurethane foams against experimental results obtained from Dawson *et al.* [15]. After validation, the model was employed to predict permeability, friction factor, Nusselt number and effective thermal conductivity of aluminum foams, highlighting the effect of the compression on these parameters.

Bai and Chung [16] simulated the flow of air in a 10 PPI foam sample of 97% porosity, employing a sphere-centered tetrakaidecahedron unit cell to represent the actual structure. They considered two types of cells, an interior cell and a boundary cell. Numerical pressure drop results were compared against experimental data from Leong and Jin [17], and good agreement was shown. The wall boundary cells experienced approximately 5% higher pressure drop than those in the interior, attributable to the no-slip condition and the larger velocity gradients at the wall. Wu *et al.* [18] simulated the interfacial heat transfer through porous ceramic foams numerically, with air as the coolant. The ceramic foams were also represented by ideally packed tetrakaidecahedron structures, and the porosity was controlled by adjusting the curvature of the blending faces. Based on the numerical simulations, a correlation was developed for predicting local and volumetric heat transfer coefficients, covering a broad range of porosities, velocities, cell sizes and temperatures [18].

There has been growing interest in the use of X-ray microtomography techniques for a variety of applications such as material characterization and reverse engineering. For example, Fiedler *et al.* [19] numerically identified defects produced during manufacturing of an open-celled metal foam. They performed finite element calculations based on microcomputed tomography data of the

samples. The effective Young's modulus and 0.2% offset yield strength were calculated, and an equivalent plastic strain was used to identify weakness within the material.

Micro computed tomography images may also be employed as the starting point for CFD analysis. Metal foams are inherently stochastic; thus, unit-cell based models only approximate the true microstructure and fail to capture the intricate details of fluid flow and heat transfer in such media. Recent advancements in computing architecture have led to increased processor speeds and memory, which enable tomography scans to be employed for mesh generation and subsequent, detailed fluid-thermal performance analysis of random porous materials such as metal foams.

Bodla *et al.* [20] adopted this approach to compute heat transfer and fluid flow parameters for aluminum foams of varying PPI, but with approximately the same relative density. The numerical results for thermal conductivity, permeability, friction factor and heat transfer coefficient were compared against experimental values and empirical correlations from the literature. The effective thermal conductivity was found insensitive to decreasing the pore size (as porosities were about the same), whereas the heat transfer coefficient and pressure drop were observed to increase as pore size was decreased.

Mendes *et al.* [21] numerically studied the effective thermal conductivity of open-celled, foam-like structures by considering different ordered structures and four real foams. They used Kelvin and cubic unit cells, and also took into account the distribution of solid phase between the struts and the nodes. Starting from the numerical results, they developed four correlations for the estimation of the effective thermal conductivity. In addition, the geometries of real open-celled foam structures were obtained from CT-scan images of two Al₂O₃-C ceramic foams and two FeCrAl-alloy metal foams, with porosities of 0.57 and 0.74, and 0.79 and 0.88, respectively. Numerical simulations were performed in order to obtain the effective thermal conductivity of the four reconstructed foams. These numerical results were compared against predictions from the correlations.

As revealed from the discussion above, there is a dearth of literature reporting one-to-one comparison of experimental and numerical results carried out on the same set of samples. In a recent study by the authors [22], a numerical analysis of pressure drop for flow of air through four reconstructed copper foam samples was performed. The results from the detailed pore-scale simulations were compared against experiments performed at the same flow rates [23] and excellent agreement was demonstrated, with mean relative and absolute global deviations of -3.8% and 5.4%, respectively. In the present study, the analysis is extended to investigate the fluid flow and the associated convective heat transfer at the pore scale, through the real structure of the same four different copper foams as considered in [22]. These foam samples have approximately the same relative density (6.4 – 6.6%), but different pore sizes (5, 10, 20, and 40 PPI). The real structures are

reconstructed from micro computed tomography images obtained at a scanning resolution of 20 μm . The computed hydraulic behavior is compared against experimental pressure drop values previously obtained on the same exact four copper foams. Similarly, the interfacial heat transfer behavior is compared against values predicted by an empirical correlation, obtained from data fitted to a large experimental database that encompasses the four samples investigated in this study.

2. METHODOLOGY

X-ray computed tomography is based on differential absorptivity of different materials to X-rays. In this technique, the object to be imaged is irradiated with X-rays and simultaneously rotated. The resulting X-ray beams are then captured via detectors, and tomographic sections of the object are reconstructed with the aid of mathematical transforms [24]. Materials with different densities show up at different grayscale values in the resultant stack of grayscale images. This technique is widely used in the field of medicine for scanning of specific areas of the body, for example for detecting tumors and bone fractures. The two-dimensional images can also be combined to produce a three-dimensional object, and may thus be employed for diagnostic or therapeutic purposes in various medical disciplines.

Industrial computed tomography (CT) scanning is now used in many areas for a variety of applications such as internal inspection of components for flaw detection, failure analysis, metrology, reverse engineering, and materials characterization. In this study, the computed tomography technique is employed for scanning four different copper foam samples, whose main characteristics are reported in Table 1; t represents the fiber thickness, l the fiber length, and a_{sv} the total available heat transfer area per unit of volume.

All of these foams are manufactured in a sandwich-like arrangement, where the foam core height is brazed between two 10 mm thick copper plates. Experimental specimens were 100 mm long and wide and 40 mm high, and were previously tested by Mancin *et al.* for their pressure drop and heat transfer performance [23].

In view of the trade-off between scan resolution and size of the sample being scanned, smaller samples were used in the scanning and subsequent numerical analysis. For this purpose, square specimens with an edge size of 15 mm were cut from the original copper samples by means of electro-erosion. This cutting technique avoids damage to the fiber ligaments, and hence the structure is scanned without introducing any defects. The cut foams, shown in Fig. 1, were scanned with a commercial X-ray μ -CT scanner at a resolution of 20 μm , with the axis along the longer

direction, *i.e.*, along the height of the foams. This resolution was chosen to enable all the microstructural details of the individual pores and ligaments to be captured.

The image-processing was performed with the commercial software Simpleware [26] employing the ScanIP module, which permits operations such as filtering, noise removal, region identification, and three-dimensional reconstruction. It also permits exporting the 3D images for CAD or mesh generation. In Fig. 2, examples of the scan images are shown for the 5, 10, 20, and 40 PPI copper foams, respectively. The strut cross sections for the investigated foam samples are observed to be mostly triangular, as was also reported by Bock and Jacobi [27]. The demarcation between the solid phase and the fluid phase is not crisp: metal absorbs X-rays leading to brighter zones, whereas air let X-rays pass, leading to darker zones. Thus, the identification of the two distinct regions (fluid and solid) is based on a threshold value. Appropriate grayscale values are identified so as to match the porosities of the reconstructed foams with those provided by the manufacturer. Further, floodfill segmentation was also performed to retain the connected ligaments, while discarding the unconnected loose ones.

At this point, since a large number of pixels would increase both the number of mesh elements and the demand on memory, a down-sampling operation was performed, such that the resolution of images is slightly lowered but the geometry is still well-represented. Representative reconstructions of the foam samples are shown in Fig. 3. According to the measurements reported in Table 1 and as can be seen from Fig. 3, the pores become smaller and the ligaments shorter and thinner as the number of pores per linear inch of the sample increases.

The foam region in the brazed regions adjacent to the copper plates at the bottom and top (see Fig. 1) was difficult to reconstruct as the presence of the copper plate created considerable noise in the scanned images. As a result, it was not possible to reconstruct the entire height of the scanned samples (40 mm). The typical reconstructed sample height was roughly 30 mm, omitting 5 mm of interface region on either side. This height is sufficient for the fluid flow computations explained in the following section.

3. NUMERICAL MODEL

The reconstructed three-dimensional foams are input to the ScanFE module in Simpleware [26] for generating finite-volume meshes. Meshing the entire scanned volume would place a significant demand on memory during mesh generation. Further, the meshes thus produced would need huge computational resources for numerical analysis of fluid flow and heat transfer. Therefore, only smaller regions were employed for mesh generation. The length of the sample in the flow direction

was 100 mm in the experiments, leading to fully developed flow. To ensure similar, fully developed flow conditions in the numerical simulations, the foam must have an adequate number of pores in the flow direction. A sensitivity analysis was carried out in order to determine the number of pores that is necessary for attaining fully developed flow. Preliminary simulations were run on the 40 PPI sample with fluid domains having the same boundary conditions and fluid properties but different number of pores along the flow direction. Domains consisting of 5, 10, and 20 pores in the flow direction were considered, and the difference in the pressure gradient determined. It was observed that the differences in the pressure gradient between the 10 pore and the 5 pore sized domains was -15.7%, whereas between the 20 pore and 10 pore sized domains, the difference was only -3.2%. A domain size of approximately 10 pores in the flow direction is therefore deemed sufficient for the flow to attain fully developed conditions for the flow speeds considered for the 10, 20, and 40 PPI samples. However, for the 5 PPI copper foam, only 6 pores were present in the flow direction as the maximum height that was possible to reconstruct was only 30 mm, as described in the previous section.

At a constant minimum mesh element size, and considering domains with 10 pores along the flow direction, the number of mesh elements directly depends on the number of pores per linear inch of the foam; the number of mesh elements increases when linear porosity decreases because the pore dimension increases, and *vice-versa*. To reduce the overall mesh count, mixed tetrahedral and hexahedral elements were employed during meshing. Table 2 presents the size of the meshed domain along with the number of elements present in the meshed volume.

Considering pore diameters of 5.08, 2.54, 1.27, and 0.635 mm for the 5, 10, 20, and 40 PPI foam, respectively, calculated as inverse PPI, there are 10 pores included along the flow direction for all the samples, except for the 5 PPI sample, for which 6 pores are included in the reconstructed height of 30 mm. The meshes are created with the ScanFE module of Simpleware [26] as noted previously.

Diani *et al.* [22] investigated pressure drop for flow of air through the copper foams by solving the continuity and momentum equations directly on the pore-scale control volume. In the present work, the analysis is extended to solve for energy transport. Following [22], the governing equations for mass, momentum and energy transport, for steady laminar incompressible flow are given by:

$$\frac{\partial}{\partial x_i} \rho u_i = 0 \quad (1)$$

$$\frac{\partial}{\partial x_i} (\rho u_j u_i) = -\frac{\partial P}{\partial x_i} + \frac{\partial}{\partial x_i} \left(\mu \frac{\partial u_i}{\partial x_j} \right) \quad (2)$$

$$\frac{\partial}{\partial x_i} (\rho u_i c_p T) = \frac{\partial}{\partial x_i} \left(\lambda \frac{\partial T}{\partial x_i} \right) \quad (3)$$

These governing equations are solved using the finite-volume commercial software ANSYS Fluent [28], using a first-order upwind difference scheme for flow and energy calculations. The SIMPLE scheme is employed for pressure-velocity coupling, and the flow field is deemed converged when the absolute value of all the residuals falls below 1.0×10^{-6} for the flow calculation, and below 1.0×10^{-7} for the thermal calculations.

As shown in Fig. 4, the following boundary conditions are employed:

- velocity-inlet boundary condition and specified temperature at the inlet of the fluid domain (y - z plane at x min);
- pressure-outlet boundary condition with zero gauge pressure at the outlet of the fluid domain (y - z plane at x max);
- symmetry boundary conditions on the lateral sides of the domain (x - y plane at z min, x - y plane at z max, x - z plane at y min, and x - z plane at y max); and
- wall with no slip boundary condition and constant heat flux at the interface between the solid and fluid domains (red areas).

The flow is assumed to be three-dimensional, steady-state, and incompressible, and the working fluid is air with constant fluid properties calculated at the mean values of temperature and pressure as reported in [23]. Further, fluid flow and heat transfer simulations were only performed in the laminar regime, with Reynolds numbers (based on the superficial velocity and on the square root of permeability [20] as the characteristic length) in the range of 62 – 215. The following section presents the details of the results obtained, as well as a comparison against experiments and empirical correlations.

4. NUMERICAL RESULTS

The experimental velocities and air properties [23] are taken as input parameters for the numerical simulations, to enable a direct comparison. A superficial velocity range of 2.5 to 5 m s⁻¹ is explored in the numerical study, with the air being at ambient pressure as in the experiments. For each sample, 6 different velocities are investigated, and the resulting numerical pressure gradients

and interstitial heat transfer coefficient are discussed. Comparisons against previously obtained experimental results are also reported.

Pore-scale simulations performed on the actual structure allow us to study the actual fluid flow and heat transfer in these intricate structures in detail. Figs. 5a and 5b present the velocity and temperature fields, respectively, for the 10 PPI sample at a cross sectional plane. These results correspond to an inlet velocity of approximately 4.9 m s^{-1} and an inlet temperature of 300 K. The metal foam ligaments act as obstacles to the flow, homogenizing the fluid flow and temperature profile, and as a result of the three-dimensional, tortuous nature of the structure, the fluid is well mixed. Local hot spot temperatures are present in the regions downstream of struts, which correspond to stagnant zones with low air velocities; however, even though the maximum air temperature rises up to 400 K, the mean air temperature remains below 330 K due to the mixing induced by such enhanced surfaces, as can be seen in Fig. 5b.

Fig. 6 compares pressure gradients from the numerical simulations against data from experiments performed at similar velocities. The pressure gradient results for the four copper foams globally match the experimental values with a mean relative and absolute deviation of -3.8% and 5.4%, respectively, demonstrating the accuracy of the novel approach employed. Relative, absolute, and standard deviations between the numerical and experimental results for each foam are summarized in Table 3.

Beginning with the converged flow field, the thermal simulations are performed by imposing a constant heat flux, q'' at the interface separating the solid and fluid regions. Thus, it is possible to calculate the numerical interfacial heat transfer coefficient, $\alpha_{numerical}$ defined as:

$$\alpha_{numerical} = \frac{q''}{\overline{T}_{wall} - \overline{T}_{air}} \quad (4)$$

In this equation, \overline{T}_{wall} and \overline{T}_{air} are the mean values of temperature for the wall and air, respectively. This numerical heat transfer coefficient is an average heat transfer coefficient because the heat flux is imposed uniformly on the entire surface.

As suggested by Mancin *et al.* [23], the interfacial heat transfer coefficient, α can be estimated as follows:

$$\alpha_{empirical} = 0.418 \cdot \text{Re}^{0.53} \cdot \text{Pr}^{1/3} \cdot \frac{\lambda_{air}}{t} \quad (5)$$

Reynolds and Prandtl numbers are defined for this equation as:

$$\text{Re} = \frac{G \cdot t}{\mu_{air} \cdot \varepsilon} \quad (6)$$

$$\text{Pr} = \frac{\mu_{air} \cdot C_{p,air}}{\lambda_{air}} \quad (7)$$

Here the thermophysical properties are calculated at the mean value of temperature and pressure. The air specific mass velocity, G , refers to the empty channel [23]. With the knowledge of the heat transfer coefficient α , it is possible to calculate the surface efficiency Ω^* , defined in [23], as:

$$\Omega^* = \frac{1 + \frac{\tanh(m \cdot L)}{m \cdot L} \cdot a_{sv} \cdot H}{1 + a_{sv} \cdot H} \quad (8)$$

Here, the foam parameters, m and L are defined as below:

$$m = \left(\frac{4 \cdot \alpha}{t \cdot \lambda_{mat}} \right)^{0.5} \cdot \left(\frac{\lambda_{mat}}{\lambda_{air}} \right)^{-0.52} \quad (9)$$

$$L = 1055 \cdot H^{1.18} \cdot \text{PPI} \cdot (0.0254 - t \cdot \text{PPI})^{0.66} \quad (10)$$

and H is the foam core height. Mancin *et al.* developed the aforementioned equations, Eq. (5)-(10) based on experimental data collected on a total of 21 metal foams, varying in terms of linear porosity (PPI), volumetric porosity, foam core height and the base material of the foam structure. Additional details regarding the derivation of foam finned surface efficiency and interfacial heat transfer coefficient may be found in [23]. It may be noted that the four copper foams under investigation in the present study were among these 21 samples, thereby enabling us to compare our

results against the developed empirical correlations. The empirical model was able to satisfactorily predict the experimental measurements within $\pm 20\%$, with a relative deviation of -1.5% , an absolute deviation of 9.6% and a standard deviation of 11.4% [23].

Fig. 7 shows the numerical results of interfacial heat transfer coefficient and foam finned surface efficiency, plotted as a function of the pore velocity for the four samples investigated. The numerically computed interfacial heat transfer coefficient, $\alpha_{numerical}$, and a foam core height H of 40 mm (height of the original specimens under investigation), is employed to calculate the foam finned surface efficiency. As may be observed, the interfacial heat transfer coefficient increases as the pore velocity or PPI of the foam are increased. Despite a larger heat transfer coefficient, the 40 PPI sample has the lowest efficiency, attributable to its thin ligaments. The foam finned surface efficiency has an opposite trend relative to the interfacial heat transfer coefficient, *i.e.*, Ω^* decreases when either the pore velocity or PPI are increased.

The comparison between numerical interfacial heat transfer coefficient and the values predicted by the correlation of Eq. (5) is reported in Fig. 8. The present numerical results are in very good agreement with their empirical counterparts and have a relative deviation of 1.6% , an absolute deviation of 9.5% , and a standard deviation of 2.7% . Fig. 9 presents a comparison between the experimental and numerical values of the interstitial heat transfer coefficient, $\alpha \cdot \Omega^*$, where $\alpha_{numerical}$ is used as heat transfer coefficient in Eq. (9) for the calculation of Ω^* numerically. The values of mean relative, absolute and standard deviations observed between the numerical and empirical results are -2.1% , 5.5% , and 4.8% , respectively. The deviations observed for each sample investigated are reported in Table 3. These results validate the numerical hydraulic and thermal analysis approaches employed in the present study and demonstrate the utility of the technique to compute detailed flow physics directly at the pore scale.

6. CONCLUSIONS

Forced convection of air through the real structure of metal foams is numerically investigated. Pore-scale structures are obtained by micro-computed tomography scanned images of four different copper foams, having about the same relative density ($6.4 - 6.6\%$) but different linear porosity (5 , 10 , 20 , and 40 PPI), with a scan resolution of $20 \mu\text{m}$. The scanned samples were reconstructed and meshed employing the commercial software Simpleware.

The hydraulic and thermal behavior of these materials was modeled with the commercial CFD analysis package, ANSYS Fluent. Experimental conditions reported in a previous work were employed as boundary conditions, to facilitate a direct comparison between numerical and

experimental values. It was observed that the numerical analysis employed in this study predicts pressure gradients very well, with a mean relative and absolute deviation of -3.8% and 5.4%, respectively. Further, the computed interstitial heat transfer coefficients are compared against values predicted by an empirical correlation from the literature. This correlation was derived from experimental measurements performed on a variety of metal foams encompassing the four foam samples investigated in the current study. Both the numerical interfacial heat transfer coefficients, and the product of interfacial heat transfer coefficient and surface efficiency, *i.e.*, interstitial heat transfer coefficient, agree well with the experimental/empirical values.

ACKNOWLEDGEMENT

The support of the Ministero dell'Istruzione, dell'Università e della Ricerca (MIUR) through the PRIN Project 2009TSYPM7_003 is gratefully acknowledged.

REFERENCES

- [1] C.Y. Zhao, Review on thermal transport in high porosity cellular metal foams with open cells, *Int. J. Heat Mass Transf.* 55 (2012) 3618-3632.
- [2] S. Mancin, C. Zilio, L. Rossetto, A. Cavallini, Heat transfer performance of aluminum foams, *J. Heat Transf.* 133 (2011) 060904-1-9.
- [3] L.B. Younis, R. Viskanta, Experimental determination of the volumetric heat transfer coefficient between stream of air and ceramic foam, *Int. J. Heat Mass Trans.* 36 (1993) 1425-1434.
- [4] J.J. Hwang, G.J. Hwang, R.H. Yeh, Measurement of interstitial convective heat transfer and frictional drag for flow across metal foams, *J. Heat Trans.* 124 (2002) 120-129.
- [5] W.H. Hsieh, J.Y. Wu, W.H. Shih, W.C. Chiu, Experimental investigation of heat transfer characteristics of aluminum-foam heat sink, *Int. J. Heat Mass. Trans.* 47 (2004) 5149-5157.
- [6] N. Dukhan, K.C. Chen, Heat transfer measurements in metal foam subjected to constant heat flux, *Exp. Therm. Fluid Sci.* 32 (2007) 624-631.
- [7] G. Incera Garrido, F.C. Patcas, S. Lang, B. Czarnetzki, Mass transfer and pressure drop in ceramic foams: A description for different pore sizes and porosities, *Chem. Eng. Sci.* 63 (2008) 5202-5217.
- [8] S. Mancin, C. Zilio, A. Diani, L. Rossetto, Experimental air heat transfer and pressure drop through copper foams, *Exp. Therm. Fluid Sci.* 36 (2012) 224-234.
- [9] T.J. Lu, H.A. Stone, M.F. Ashby, Heat transfer in open-cell metal foams, *Acta Mater.* 46 (1998) 3619-3635.
- [10] K. Boomsma, D. Poulikakos, Y. Ventikos, Simulations of flow through open cell metal foams using an idealized periodic cell structure, *Int. J. Heat Fluid Flow* 24 (2003) 825-834.
- [11] K. Brakke, *The Surface Evolver*, *Exp. Math.* 1 (1992) 141-165.
- [12] K. Boomsma, D. Poulikakos, The effects of compression and pore size variations on the liquid flow characteristics of metal foams, *J. Fluids Eng.* 124 (2002) 263-272.
- [13] S. Krishnan, S.V. Garimella, J.Y. Murthy, Simulation of thermal transport in open-cell metal foams: Effects of periodic unit-cell structure, *J. Heat Trans.* 130 (2008) 024503-1-5.
- [14] R. Ravi Annapragada, J.Y. Murthy, S.V. Garimella, Permeability and thermal transport in compressed open-celled foams, *Num. Heat Transf. Part B: Fundamentals* 54 (2008) 1-22.
- [15] M.A. Dawson, J.T. Germaine, L.J. Gibson, Permeability of open-cell foams under compression strain, *Int. J. Solids Struct.* 44 (2007) 5133-5145.

- [16] M. Bai, J.N. Chung, Analytical and numerical prediction of heat transfer and pressure drop in open-cell metal foams, *Int. J. Therm. Sci.* 50 (2011) 869-880.
- [17] K.C. Leong, L.W. Jin, Effect of oscillatory frequency on heat transfer in metal foam heat sink of various pore densities, *Int. J. Heat Mass Transf.* 49 (2006) 671-681.
- [18] Z. Wu, C. Caliot, G. Flamant, Z. Wang, Numerical simulation of convective heat transfer between air flow and ceramic foams to optimize volumetric solar air receiver performance, *Int. J. Heat Mass Tran.* 54 (2011) 1527-1537.
- [19] T. Fiedler, I.V. Belova, G.E. Murch, μ -CT-based finite element analysis on imperfections in open-cell metal foam: Mechanical properties, *Scripta Mater.* 67 (2012) 455-458.
- [20] K.K. Bodla, Y.M. Murthy, S.V. Garimella, Microtomography-based simulation of transport through open-cell metal foams, *Numer. Heat Transf. Part A* 58 (2010) 527-544.
- [21] M.A.A. Mendes, S. Ray, D. Trimis, A simple and efficient method for the evaluation of effective thermal conductivity of open-cell foam-like structures, *Int. J. Heat Mass Tran.* 66 (2013) 412-422.
- [22] A. Diani, K.K. Bodla, L. Rossetto, S.V. Garimella, Numerical analysis of air flow through meta foams, *Energy Procedia* 45 (2014) 645-652.
- [23] S. Mancin, C. Zilio, A. Diani, L. Rossetto, Air forced convection through metal foams: Experimental results and modeling, *Int. J Heat Mass Trans.* 62 (2013) 112-123.
- [24] L.A. Feldkamp, L.C. Davis, J.W. Kress, Practical cone-beam algorithm, *J. Opt. Soc. Am. A* 1 (1984) 612-619.
- [25] ERG Material and Aerospace Inc. Auckland CA, Web site www.ergaerospace.com.
- [26] Simpleware Ltd, 2012, Exeter, UK.
- [27] J. Bock, A.M. Jacobi, Geometrical Classification of open-cell metal foams using X-ray micro-computed tomography, *Mater. Charact.* 78 (2013) 35-43.
- [28] ANSYS Fluent 13, 2010.

TABLE CAPTIONS

Table 1. Geometrical characteristics of the four copper foam samples.

Table 2. Domain sizes and number of mesh elements in a typical volume employed for analysis.

Table 3. Difference between numerically computed and empirical/experimental values of $\Delta p/L$, α and $\alpha \cdot \Omega^*$. Experimental values are borrowed from Mancin *et al.* [23].

FIGURE CAPTIONS

Figure 1: Copper foam slabs (40, 20, 10, and 5 PPI, respectively).

Figure 2: Representative two-dimensional scan images, shown for: (a) 5 PPI, (b) 10 PPI, (c) 20 PPI, and (d) 40 PPI, respectively.

Figure 3: Examples of reconstructed foams. Images correspond to: (a) 5 PPI, (b) 10 PPI, (c) 20 PPI, and (d) 40 PPI, respectively.

Figure 4: Boundary conditions employed in the present study.

Figure 5: a) Velocity field contours, and b) temperature contours shown for the case of an inlet velocity of 4.9 m s^{-1} and imposed heat flux of 10 kW m^{-2} , in a cross section for the 10 PPI foam sample.

Figure 6: Comparison between numerical and experimental pressure gradients from [23].

Figure 7: Numerically computed values of (a) interfacial heat transfer coefficient, and (b) foam finned surface efficiency, shown plotted against the pores velocity for the 4 copper foam samples.

Figure 8: Computed interfacial heat transfer coefficient values for the four samples, and comparison against empirical results from [23].

Figure 9: Product of interfacial heat transfer coefficient and foam finned surface efficiency for the four samples investigated. Present computations and comparison against values from Mancin *et al.* [23].

Table 1. Geometrical characteristics of the four copper foam samples.

Sample	PPI [item in ⁻¹]	Porosity [-]	t [mm]	l [mm]	a_{sv} [m ² m ⁻³]
Cu-5-6.5	5 ^a	0.935 ^a	0.495 ^b	1.890 ^b	292 ^a
Cu-10-6.6	10 ^a	0.934 ^a	0.432 ^b	1.739 ^b	692 ^a
Cu-20-6.5	20 ^a	0.935 ^a	0.320 ^b	1.402 ^b	1134 ^a
Cu-40-6.4	40 ^a	0.936 ^a	0.244 ^b	0.999 ^b	1611 ^a

^a Measured by the manufacturer [25]

^b Measured by Mancin *et al.* [23]

Table 2. Domain sizes and number of mesh elements in a typical volume employed for analysis.

Sample	Size [mm×mm×mm]	N° mesh elements
Cu-5-6.5	9.92×9.92×29.96	~27 million
Cu-10-6.6	5.96×5.96×25.36	~10 million
Cu-20-6.5	4.40×4.40×12.76	~5 million
Cu-40-6.4	4.48×4.48×6.34	~3 million

Table 3. Difference between numerically computed and empirical/experimental values of $\Delta p/L$, α and $\alpha\Omega^*$. Experimental values are borrowed from Mancin *et al.* [23].

Parameter	Sample	e_{rel} [%]	e_{abs} [%]	σ_N [%]
$\Delta p/L$	Cu-5-6.5	2.1	2.2	1.9
	Cu-10-6.6	-14.6	14.6	0.6
	Cu-20-6.5	-2.7	2.8	1.6
	Cu-40-6.4	-0.4	2.4	1.9
α	Cu-5-6.5	-7.7	7.7	1.4
	Cu-10-6.6	-8.6	8.6	2.2
	Cu-20-6.5	8.2	8.2	0.8
	Cu-40-6.4	13.0	13.0	2.1
$\alpha\Omega^*$	Cu-5-6.5	-14.0	14.0	0.8
	Cu-10-6.6	4.0	4.0	2.4
	Cu-20-6.5	1.8	1.8	0.3
	Cu-40-6.4	-2.3	3.6	2.8

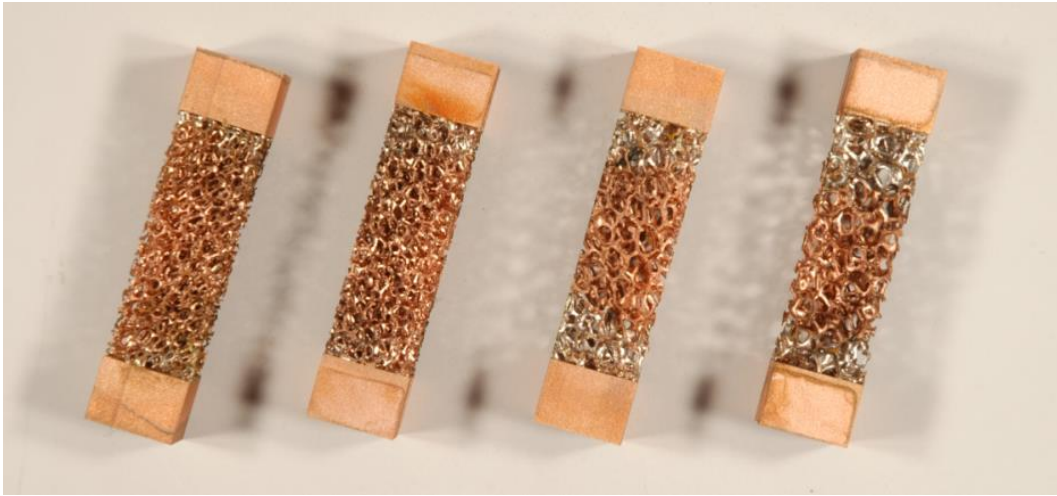


Figure 1: Copper foam slabs (40, 20, 10, and 5 PPI, respectively).

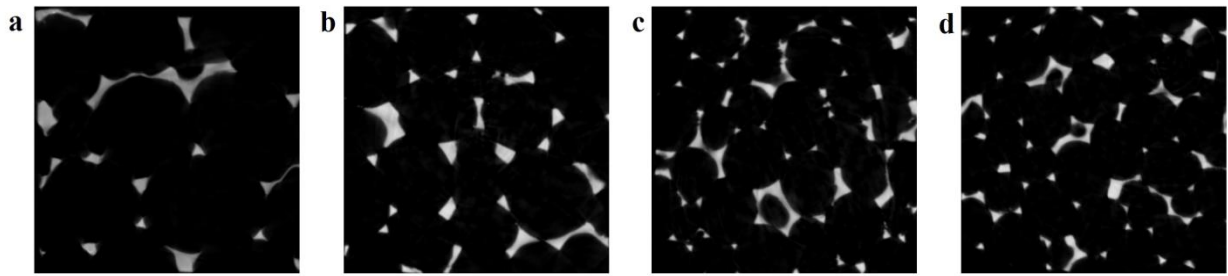


Figure 2: Representative two-dimensional scan images, shown for: (a) 5 PPI, (b) 10 PPI, (c) 20 PPI, and (d) 40 PPI, respectively.

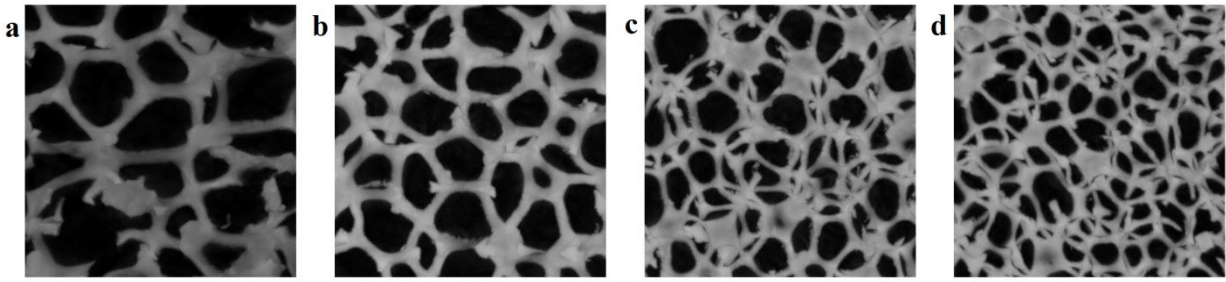


Figure 3: Examples of reconstructed foams. Images correspond to: (a) 5 PPI, (b) 10 PPI, (c) 20 PPI, and (d) 40 PPI, respectively.

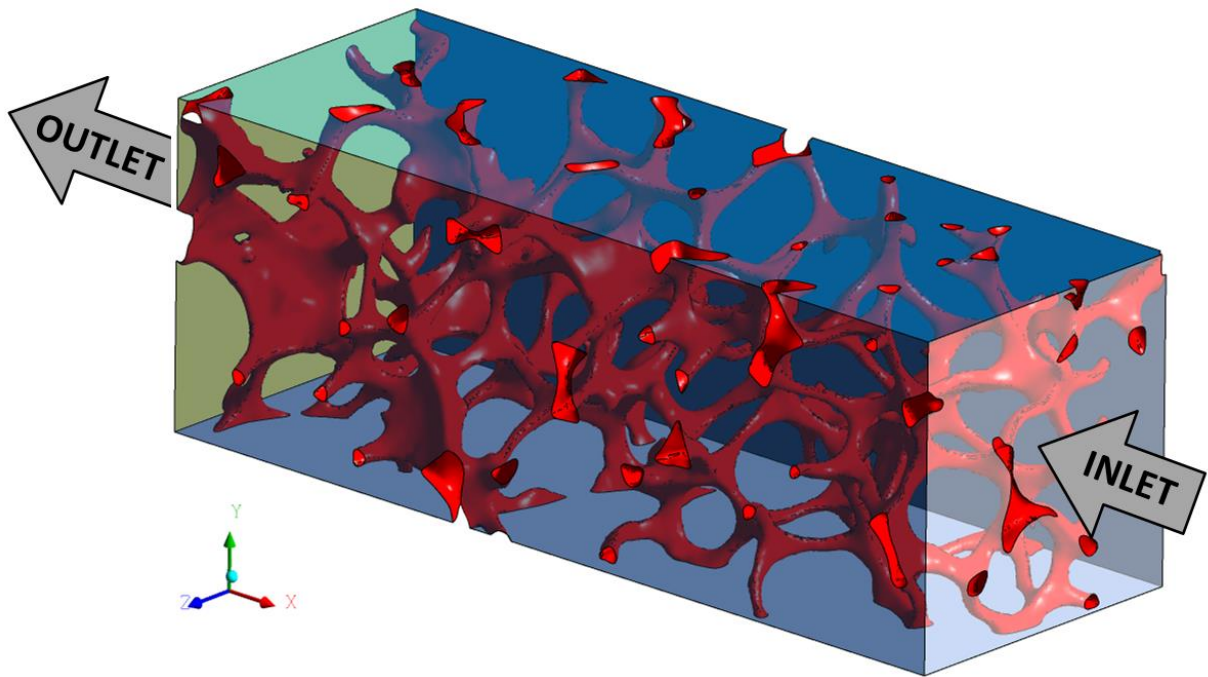


Figure 4: Boundary conditions employed in the present study.

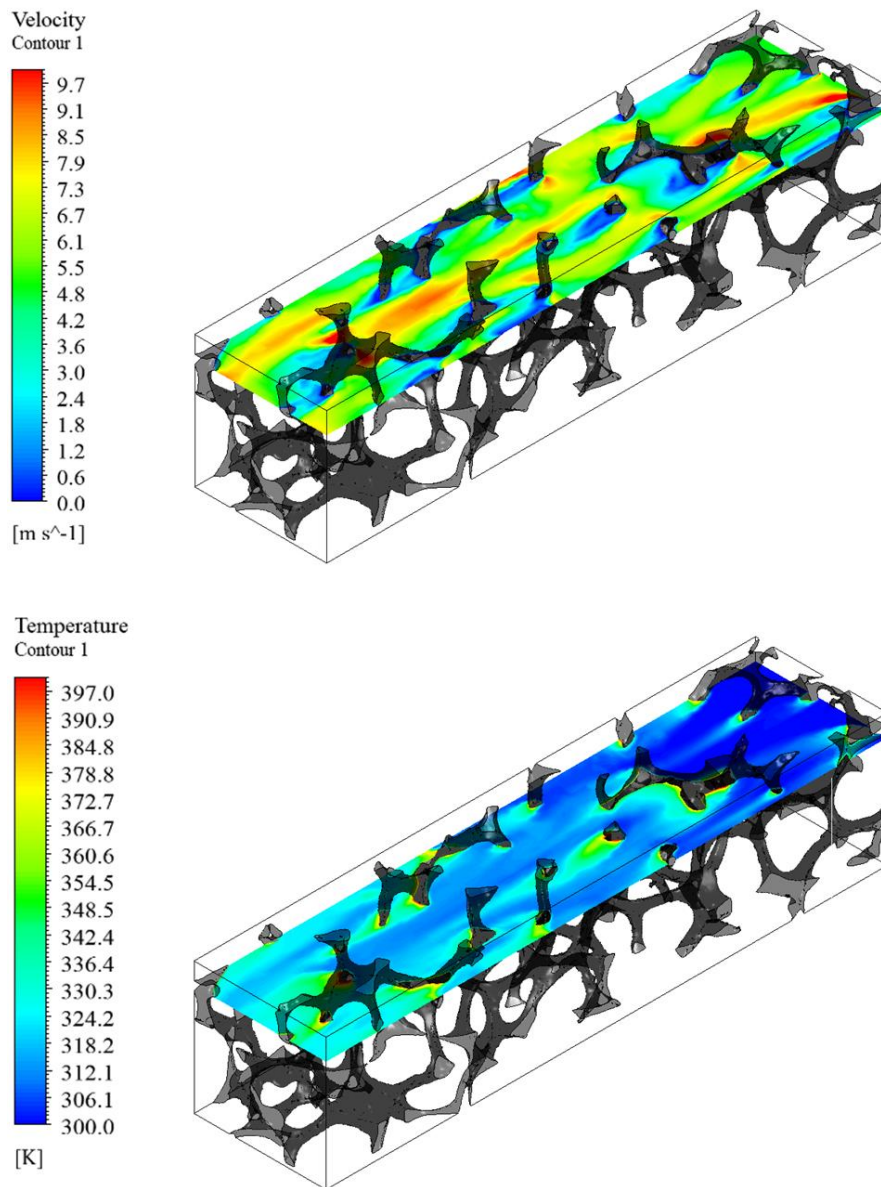


Figure 5: a) Velocity field contours, and b) temperature contours, shown for the case of an inlet velocity of 4.9 m s^{-1} and imposed heat flux of 10 kW m^{-2} in a cross section for the 10 PPI foam sample.

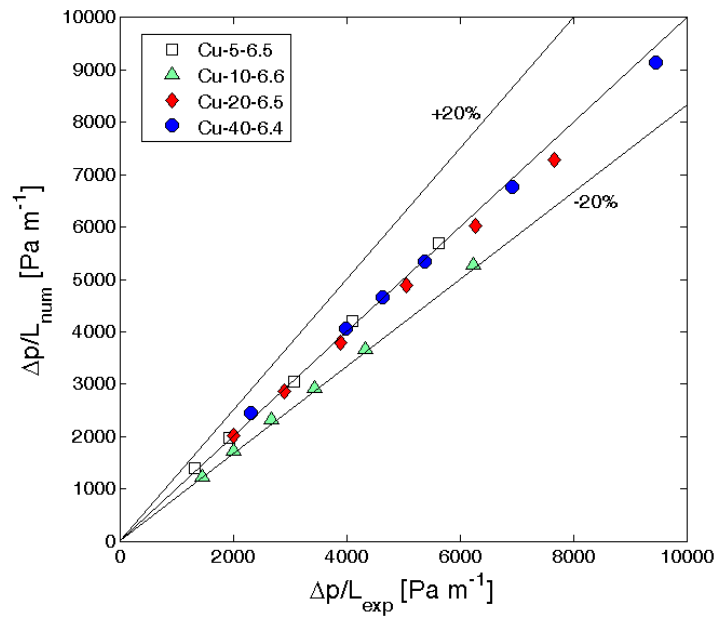


Figure 6: Comparison between numerical and experimental [23] pressure gradients.

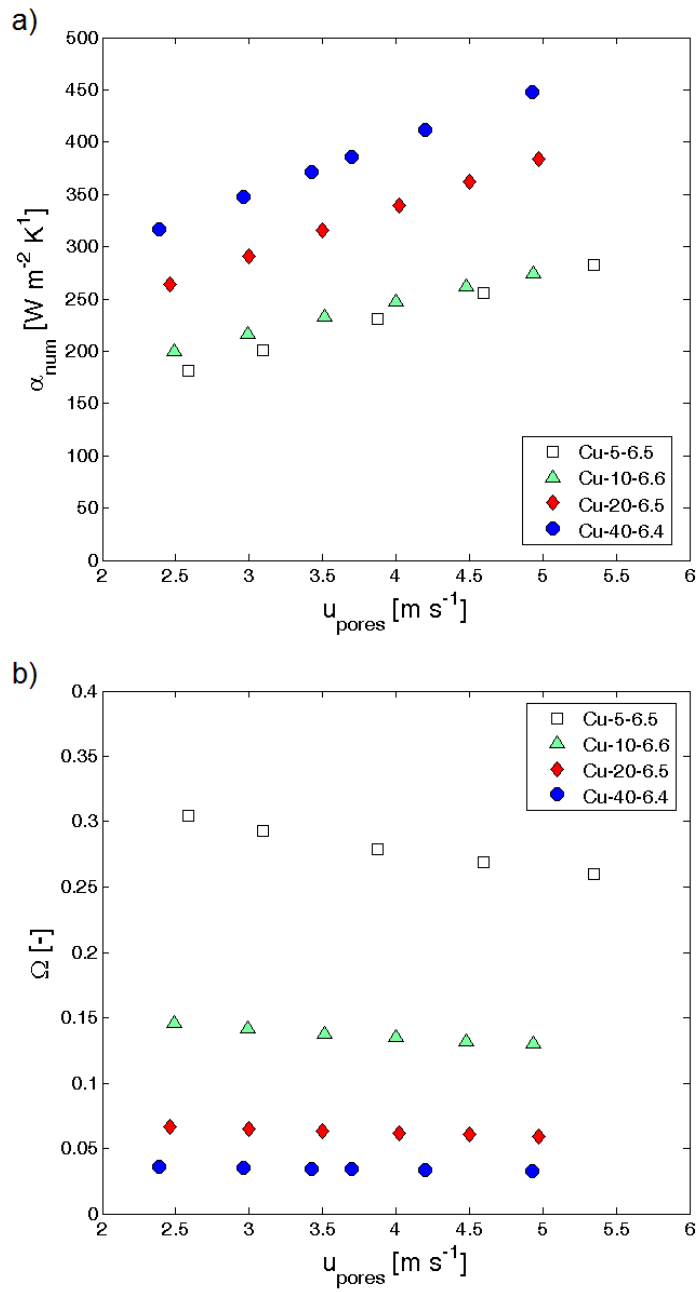


Figure 7: Numerically computed values of (a) interfacial heat transfer coefficient, and (b) foam finned surface efficiency, shown plotted against the pores velocity for the 4 copper foam samples.

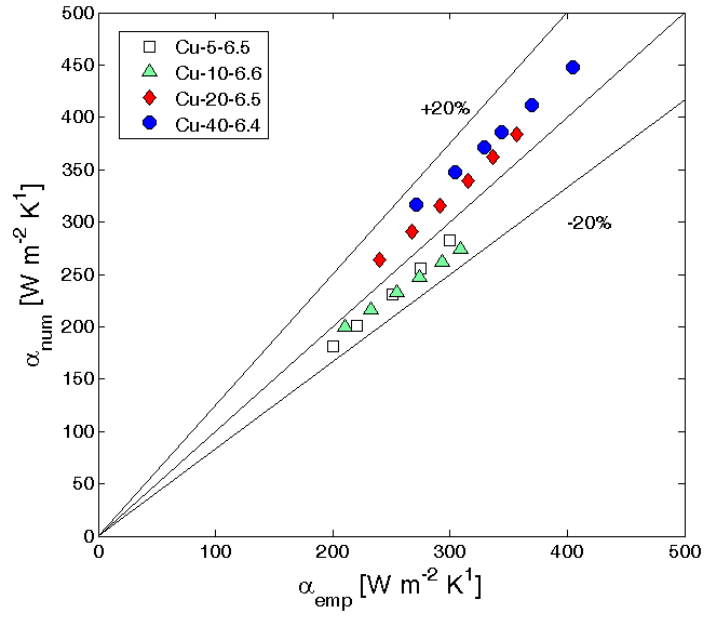


Figure 8: Computed interfacial heat transfer coefficient values for the four samples, and comparison against empirical [23] results.

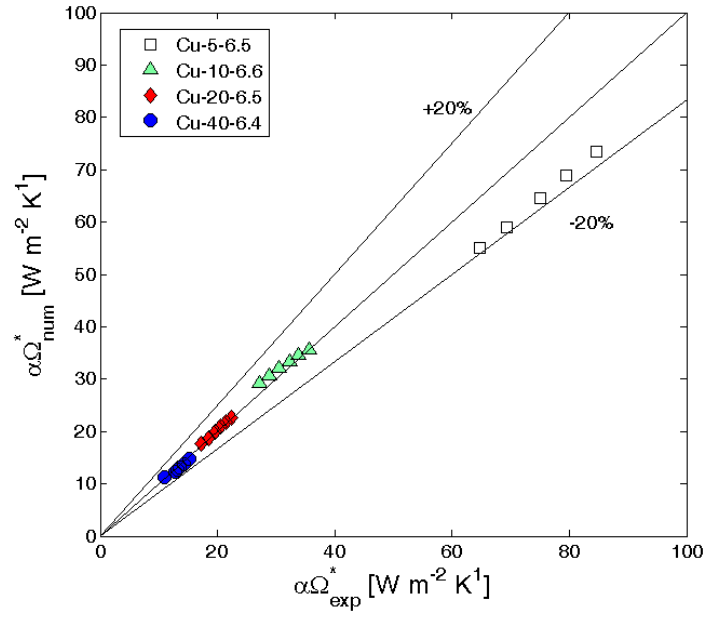


Figure 9: Product of interfacial heat transfer coefficient and foam finned surface efficiency for the four samples investigated. Present computations and comparison against values from Mancin *et al.* [23].